Submitted to *Inorg. Chem.*, July 2013 – Revised October 2013

Electronic Supporting Informations

Investigation on NMR Relaxivity of Nano-Sized Cyano-Bridged Coordination Polymers.

Marine Perrier,[a] Samir Kenouche,[b] Jêrôme Long,[a] Kalaivani Thangavel,[c] Joulia Larionova,*[a] Christophe Goze-Bac,[b] Alessandro Lascialfari,[c, d] Manuel Mariani,[e] Nathalie Baril,[f] Christian Guérin,[a] Bruno Donnadieu,[g] Alexander Trifonov,[h] and Yannick Guari[a]

[a]*Institut Charles Gerhardt Montpellier, UMR 5253 CNRS-UM2-ENSCM-UM1, Chimie Moléculaire et Organisation du Solide, Université Montpellier II, Place E. Bataillon, 34095 Montpellier cedex 5, France. Fax: (33)467143852, e-mail: joulia.larionova@univ-montp2.fr.*

[b]*Laboratoire Charles Coulomb (L2C) BioNanoNMRI UMR 5221, Université Montpellier 2, France*

[c]*Dipartimento di Fisica and INSM,, Università degli studi di Milano, I-201334 Milano, Italy.*

[d]*Centro S3, CNR-Istituto di Nanoscienze, I-41125 Modena, Italy*

[e]*Dipartimento di Fisica e Astronomia, Università degli studi di Bologna, 40126 Bologna (Italy)*

[f]*Fédération de recherche 3C, FR 3512, CNRS-Aix-Marseille Université, 3 place Victor Hugo, 13331 Marseille cedex 3, France*

[g]*Fédartion de Recheche Chimie Balard – FR3105, Université Montpellier II, Place E. Bataillon, 34095 Montpellier cedex 5, France*

[h]*G. A. Razuvaev Institute of Organometallic Chemistry of the Russian Academy of Science, Tropinina 49, GSP-44S, 603950, Nizhny Novgorod, Russia.*

Table S1. Some relevant characteristics of the samples **5**–**7**.

Sample	Composition	M^{n+}/M'^{m+} ratio[a]	IR, ν(CN), cm^{-1}	Nanoparticle size,[b] nm	Lattice Parameter, Å
5	$Ni^{2+}/[Fe(CN)_6]^{3-}$@PEG1000	1.48	2167, 2119	3.0 ± 0.4	*fcc,* 10.16
6	$Cu^{2+}/[Fe(CN)_6]^{3-}$@PEG1000	1.45	2170, 2115	5.5 ± 0.6	*fcc,* 10.30
7	$Fe^{2+}/[Fe(CN)_6]^{3-}$@$PEGNH_2$	-	2075	1.4 ± 0.4	*fcc,* 10.15

Structural description of $Gd(H_2O)_4[Fe(CN)_6]$

The compound crystallizes in the orthorhombic system with a *Cmcm* space group and cell parameters equal to *a* = 7.4016(3) **Å**, *b* = 12.7813(14) **Å** and *c* = 13.5980(12) **Å.** The asymmetric unit is composed of two crystallographically independent ions, Gd^{3+} and Fe^{3+}. The coordination sphere of the Gd^{3+} centers (in violet) is constituted of six nitrogen belonging to cyanide groups plus two coordinated water molecules leading to a $\{GdN_6O_2\}$ environment describing a slightly distorted square antiprism with the Ln–(N,O) bond lengths ranging from 2.363(1) to 2.495(2) Å (Figure 1b). Such coordination geometry is characteristic for Gd^{3+} ion.[1] The coordination environment of the Fe^{3+} ions consists of six carbon atoms from six cyano-ligands leading to an octahedral geometry. Intermetallic connectivity is achieved *via* the μ_2-cyanide bridges, ultimately leading to the formation of the neutral three-dimensional $_\infty^3[Gd(H_2O)_2Fe(CN)_6]\bullet 2H_2O$ network (Figure 1a). The connectivity between three gadolinium(III) and six iron(III) metallic ions creates distorted pores having an approximate dimension of 7.40 Å × 5.35 Å × 7.38 Å and containing two crystallized waters (Figure 1c). Highly strong and directional hydrogen bonds ($d_{O\cdots O}$ = 2.802(2); angle O-H···O = 169.43°) appear between crystallized and coordinated water molecules forming a cluster of four water molecules inside the pore.

Crystallographic data are presented in Table S2. A single crystal of $Gd(H_2O)_4[Fe(CN)_6]$ was mounted on a glass fiber and measured at low temperature T = 173 K under nitrogen gaz. X-ray measurements were made using a Agilent, Xcalibur four circles kappa geometry diffractometer equipped with a Agilent Sapphire2, large Be window CCD area-detector using a Mo-K_α monochromatized radiation (λ = 0.71073 Å) .[2] Intensities were integrated from several series of exposures, and the total data set being a sphere. An empirical absorption correction was applied, using spherical harmonics, implemented in SCALE3 ABSPACK scaling algorithm.[3] The structure was solved by direct methods[4] and subsequent differences Fourier maps, then refined by least squares procedures on weighted F^2 values using SHELXL-97[5] included in the WinGx system programs for Windows.[6] All non-hydrogen atoms were assigned anisotropic displacement parameters and refined without positional constraints. Hydrogen atoms were constrained to ideal geometries and refined with fixed isotropic displacement parameters. Least squares refinement proceeded smoothly to give the residuals shown in Table S2.

Table S2. Crystal data and structure refinement for $Gd(H_2O)_4[Fe(CN)_6]$.

Empirical formula	$C_6H_8FeGdN_6O_4$	
Formula weight	441.28	
Temperature	173(2) K	
Wavelength	0.71073 Å	
Crystal system	Monoclinic	
Space group	C m c m	
Unit cell dimensions	a = 7.4016(3) Å	α = 90°
	b = 12.7813(14) Å	β = 90°
	c = 13.5980(12) Å	γ = 90°
Volume	1286.40(19) $Å^3$	
Z	4	
Density (calculated)	2.279 mg/m^3	
Absorption coefficient	6.254 mm^{-1}	
F(000)	832	
Crystal size	0.28 x 0.10 x 0.08 mm	
θ range for data collection	3.15 to 32.5°	
Index ranges	-8<=h<=8, -19<=k<=19, -22<=l<=22	
Reflections collected	4090	
Independent reflections	1161 [R_{int} = 0.0213]	
Completeness to □ = 32.5°	89.7 %	
Absorption correction	Empirical correction	
Max. and min. transmission	0.2734 and 0.6346	
Refinement method	Full-matrix least-squares on F^2	
Data / restraints / parameters	1161 / 0 / 52	
Goodness-of-fit on F^2	S = 1.134	
R indices [for 2890 reflections with I>2□(I)]	R_1 = 0.0164, wR_2 = 0.0364	
R indices (for all 3693 data)	R_1 = 0.0179, wR_2 = 0.0367	
Weighting scheme	'calc w=1/[\s^2(Fo^2) + (0.0127P)^2 + 2.4921P]	
where P=(Fo^2 + 2Fc^2)/3'		
Refine_ls_extinction_coef	0.00087(11)	
Refine_ls_extinction_expression		
'Fc*=kFc[1+0.001xFc^2\l3/sin(2\q)]$^{-1/4}$,		
Largest diff. peak and hole	0.646 and -0.535 eÅ	

Table S3. Vogel-Fulcher law fits applied to the dynamic behavior for nanoparticles **5** – **7.**

Référence	Vogel Fulcher law's parameters			
	T_{max}, K	τ_0, s	E_a/k_B, K	T_0, K
5	20.0	$1.16 \cdot 10^{-12}$	96.68	12.55
6	9.99	$3.47 \cdot 10^{-12}$	97.50	6.5
7	1.9	$5.65 \cdot 10^{-11}$	25.6	0.34

Table S4. Relaxivity and magnetic properties for samples **5** – **7**. The relaxivities values obtained at 300 K under a 4.7 T applied magnetic field.

Sample	Composition	r_1, $s^{-1}.mM^{-1}$	r_2, $s^{-1}.mM^{-1}$	r_2/r_1	$\chi T_{calc.}$ emu.K.mol^{-1} [a]	χT_{exp}, emu.K.mol^{-1} [b]
	ProHance® (Gadoteridol)	3.5±0.1	5.4±0.1	1.53	7.875	-
5	$Ni^{2+}/[Fe(CN)_6]^{3-}$@PEG1000	0.08[a]	1.32[a]	16.50	3.75	3.00
6	$Cu^{2+}/[Fe(CN)_6]^{3-}$@PEG1000	0.26[a]	1.09[a]	4.19	1.875	1.45
7	$Fe^{3+}/[Fe(CN)_6]^{4-}$@$PEGNH_2$	0.09± 0.01	2.05 ± 0.01	21.57	13.12	10.95

[a] calculated based on the bulk compounds $M_3[Fe(CN)_6]_2 \cdot 15H_2O$, $Fe_4[Fe(CN)_6]_3 \cdot 15H_2O$

[b] measured at 300 K at 60 mHz.

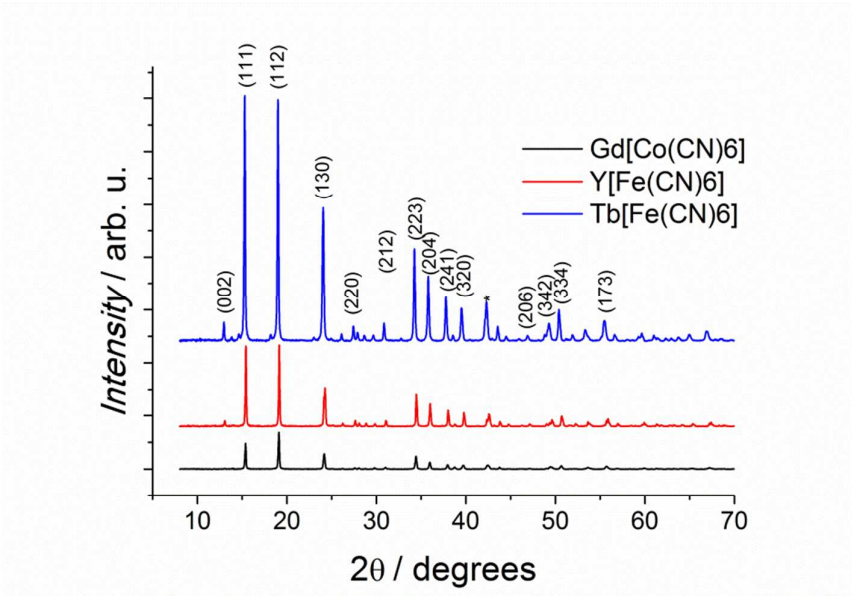

Figure S1. Room temperature PXRD patterns for $Gd^{3+}/[Co(CN)_6]^{3-}$@PEG400 (**2**), and $Y^{3+}/[Fe(CN)_6]^{3-}$@PEG400 (**4**) and $Tb^{3+}/[Fe(CN)_6]^{3-}$@PEG400 (**3**).

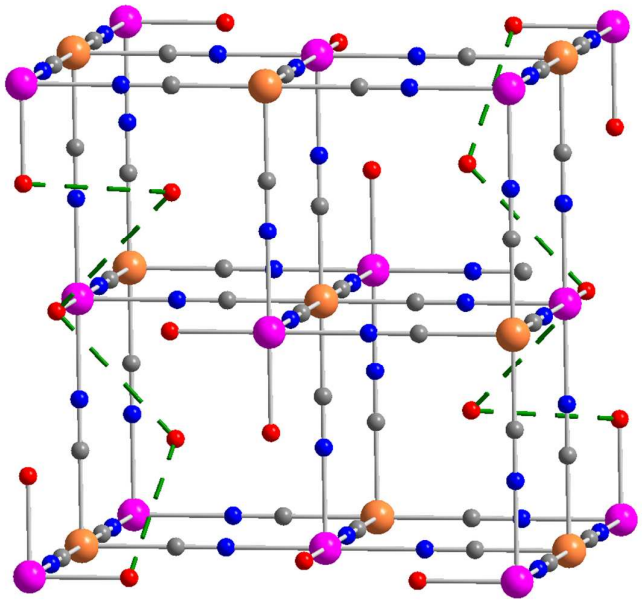

Figure S2. Representation of a lacunary Prussian Blue analogue structure showing the hydrogen bonding network (green dashed lines) between coordinated and zeolitic water molecules.

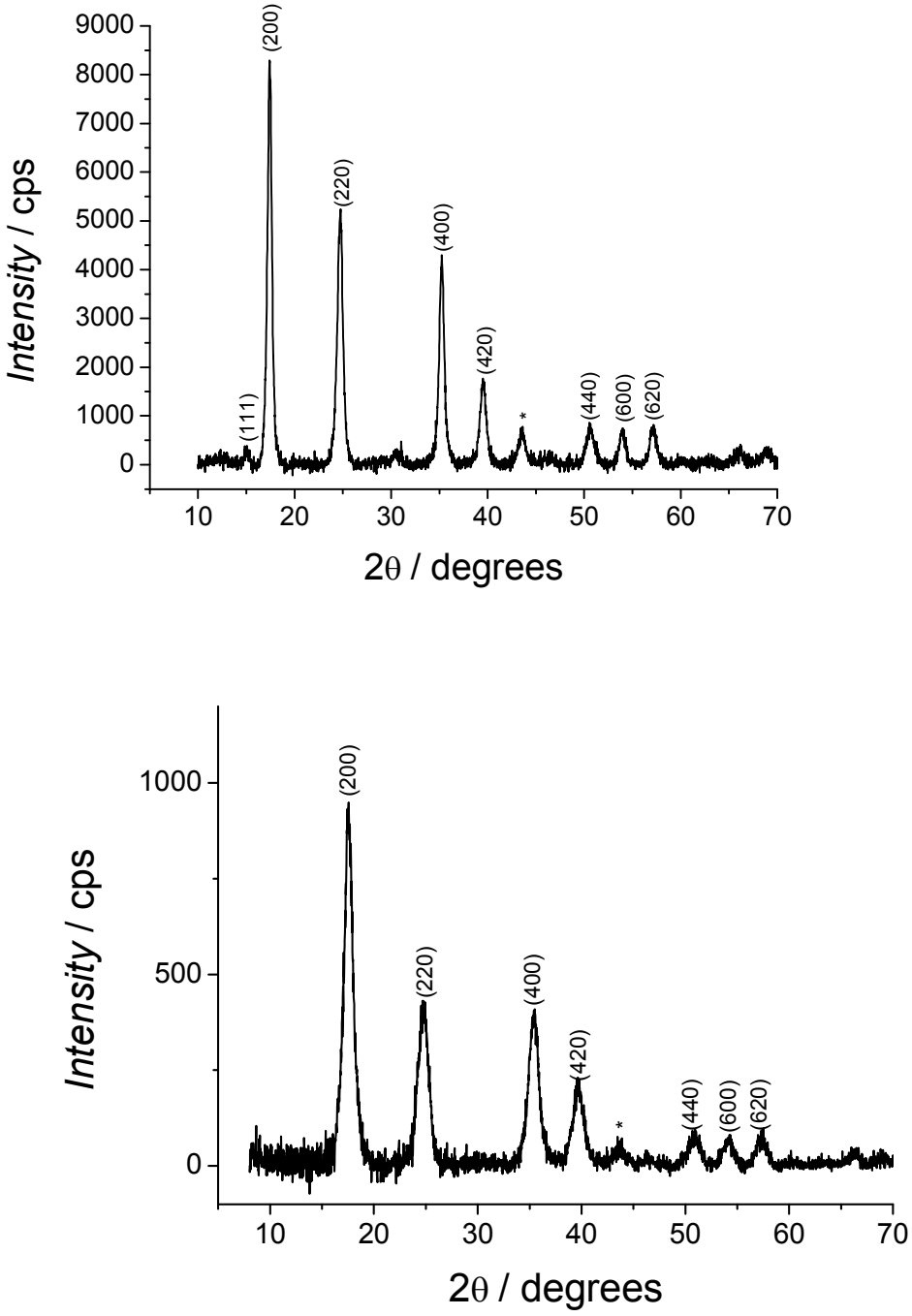

Figure S3. Room temperature PXRD pattern for (top) $Ni^{2+}/[Fe(CN)_6]^{3-}$@PEG1000 **5** indexed with the space group *Fm-3m* and (down) $Fe^{3+}/[Fe(CN)_6]^{4-}$@PEGNH_2.

.

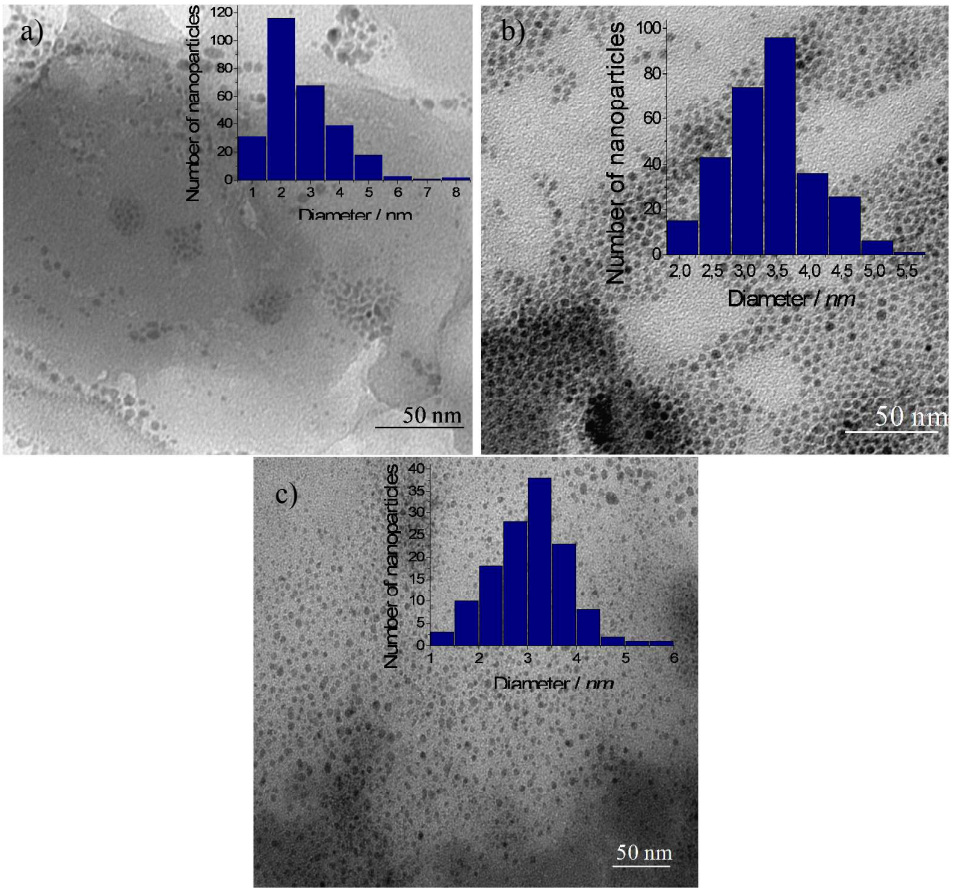

Figure S4. TEM image of nanoparticles and the corresponding histograms of the nanoparticle's size distribution (inset) for a) $Gd^{3+}/[Fe(CN)_6]^{3-}$@$PEGNH_2$ **1c**; b) $Gd^{3+}/[Fe(CN)_6]^{3-}$@NADG **1d;** c) $Y^{3+}/[Fe(CN)_6]^{3-}$@PEG400 **4**.

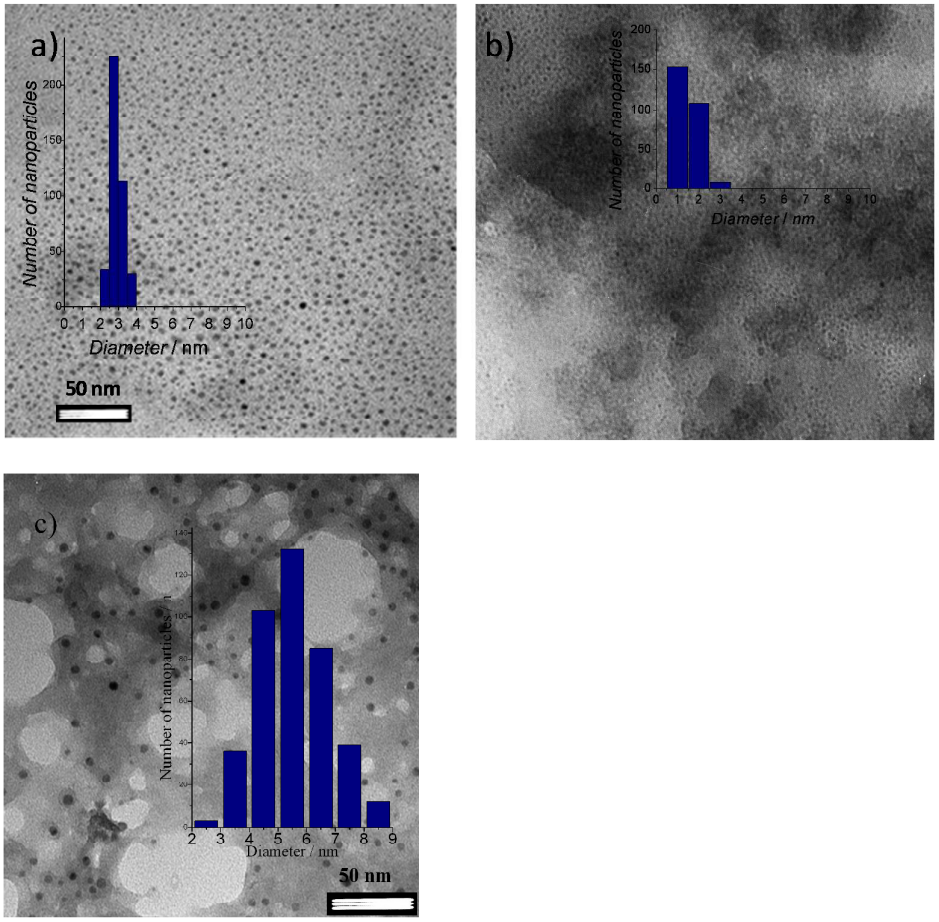

Figure S5. TEM image of nanoparticles and the corresponding histograms of the nanoparticle's size distribution (inset) for : a) $Ni^{2+}/[Fe(CN)_6]^{3-}$@PEG1000 5, b) $Fe^{3+}/[Fe(CN)_6]^{4-}$@$PEGNH_2$ 7 and c) $Cu^{2+}/[Fe(CN)_6]^{3-}$@PEG1000 6.

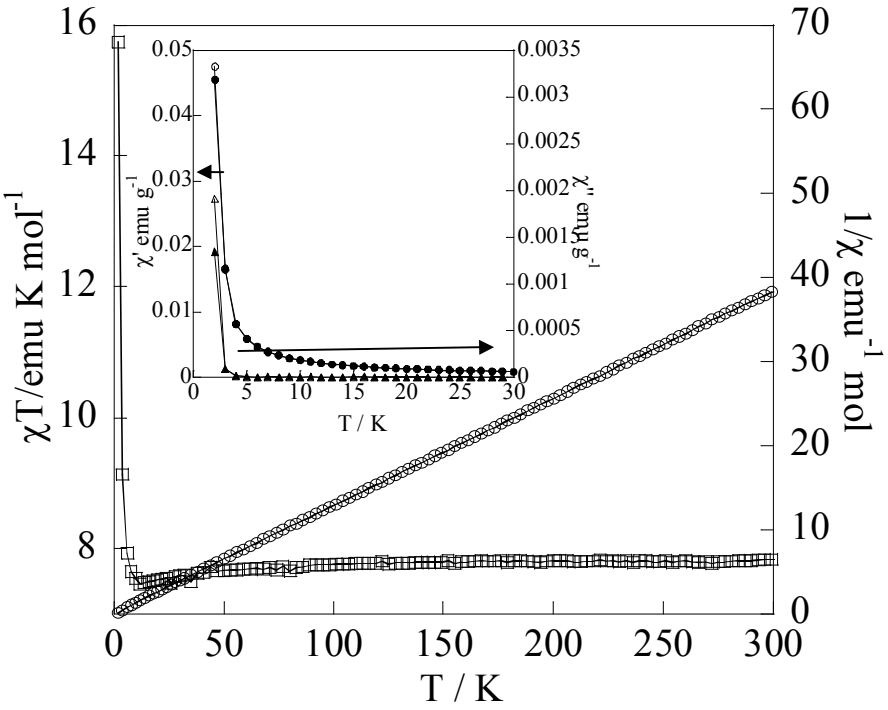

Figure S6. Temperature dependence of χT (□) and $1/\chi$ (o) for $Gd^{3+}/[Fe(CN)_6]^{3-}$@PEG1000 **1b** with an applied magnetic field of 1000 Oe. Inset: Temperature dependence of the in-phase (χ') and of out-of-phase (χ'') components of the ac susceptibility with zero dc magnetic field for $Gd^{3+}/[Fe(CN)_6]^{3-}$@PEG1000 **1b**.

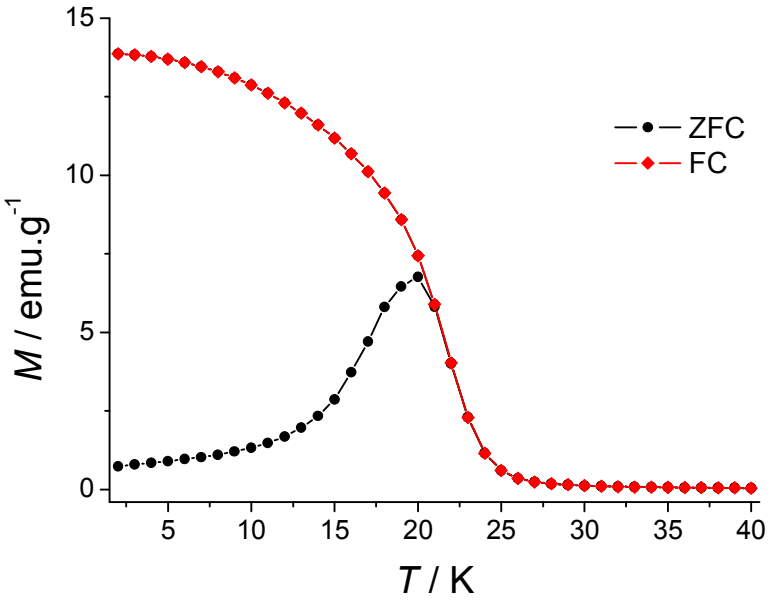

Figure S7. ZFC/FC magnetization curves collected for **5** with an applied magnetic field of 100 Oe.

Description of low temperature magnetic properties:

The zero field-cooled (ZFC) / field-cooled (FC) magnetization curves measured in the temperature range 2 – 25 K for **5** are given as an example Figure 7S. In the ZFC experiment, the sample is cooled in the absence of a static magnetic field and the magnetization is then recorded as a function of temperature under a 100 Oe field. The FC magnetization data were then collected after cooling the sample in the same magnetic field. The ZFC curve shows a narrow peak at T_{max} = 20.0 K, while the FC curve increases with decreasing temperature and tends to saturation. This increase of the FC curve is usually interpreted as the signature of nanoparticles presenting interparticle dipolar interactions.[7] The FC and ZFC curves coincide at high temperatures and start to separate at 22 K. The closeness of the ZFC maximum temperature and the ZFC/FC separation temperature attests a very narrow size distribution of the nanoparticles. The temperature dependence of χ' and χ'' components of the ac susceptibility for **5** was measured in a zero static field in the 1 - 1500 Hz range (Figure S8). At 10 Hz, χ' and χ'', exhibit peaks at 17.75 and 16.70 K, respectively, which shift to higher temperature increasing the frequency. The analysis of the frequency dependence of the relaxation time using the Arrhenius law, $\tau = \tau_0 \exp(E_a/k_B T)$, leads to parameters without physical meanings: $\tau_0 = 2.65 \cdot 10^{-53}$ s and E_a = 1946 K. One has to notice that the small value of

τ_0, generally expected in the 10^{-8}-10^{-12} s range for superparamagnetic systems, implies strong interaction among the nanoparticles. In fact, the calculated Mydosh parameter, $\varphi = (T_{max} - T_{min})/(T_{max} \times(\log \nu_{max} - \log \nu_{min})) = 0.020$,[8] is lower than the value commonly observed for superparamagnets (> 0.1), a situation that is usually attributed to the existence of strong interactions (of dipole-dipole origin) between the nanoparticles. The temperature dependence of the relaxation time can be described with the Vogel-Fulcher law, $\tau = \tau_0 exp(E_a/k_B(T-T_0))$, where the additional parameter T_0 indicates the strength of interparticle interactions. The obtained values of E_a/k_B, τ_0 and T_0 are equal to 96.68 K, 1.16×10^{-12} s and 12.55 K, respectively, and correspond to what is observed for the classical spin-glass systems confirming the presence of interparticle interactions at low temperature (Figure S9). The nanoparticles **6** and **7** present a similar spin-glass magnetic behavior at low temperature (Table S3, ESI).

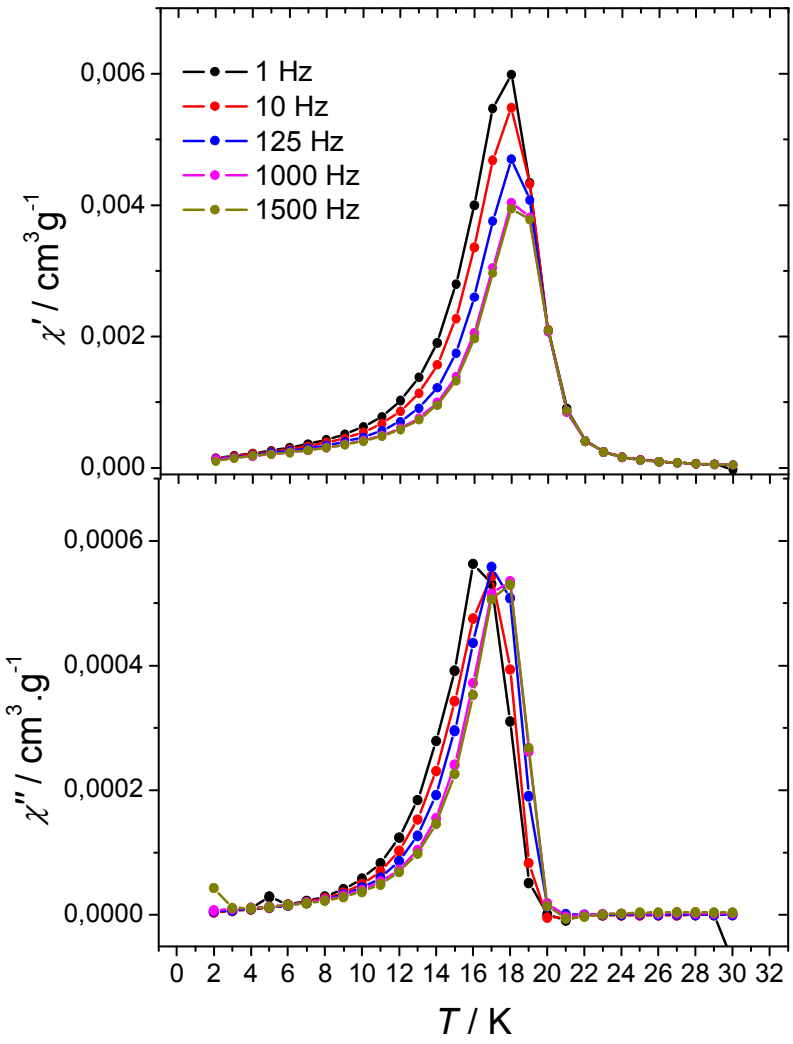

Figure S8. Temperature dependence of in-phase χ' (top) and of out-of-phase χ'' (bottom) components of the ac susceptibility with zero dc magnetic field for **5**.

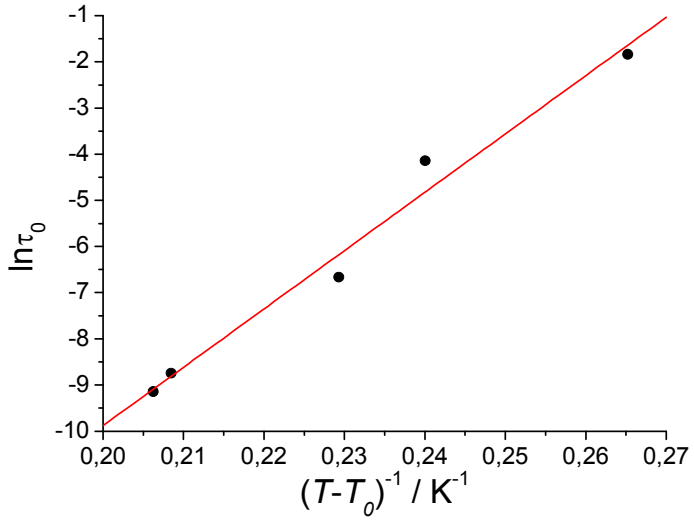

Figure S9. The relaxation time dependence with frequency fitted with the Vogel–Fulcher law, $\tau = \tau_0 \exp(E_a/k_B(T - T_0))$ for **5**.

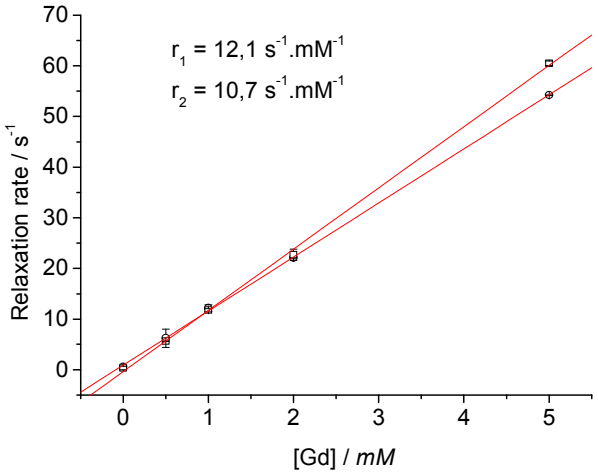

Figure S10. a) T_1 and b) T_2 relaxation rate measurements *vs* concentration of aqueous solutions of the nanoparticles **1a** performed at an applied magnetic field of 7 T.

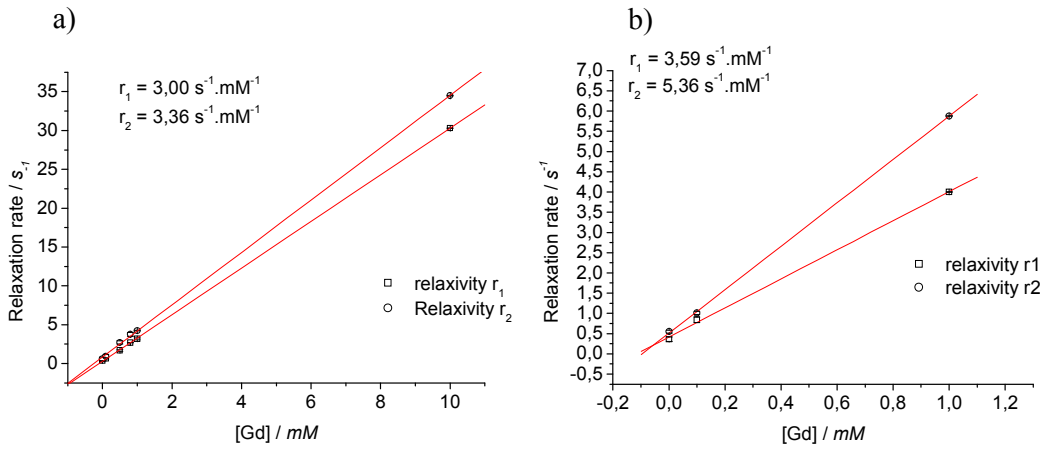

Figure S11. T_1 and T_2 relaxation rate measurements *vs* concentration of aqueous solutions of the Gadoteridol (ProHence) commercial CA performed at an applied magnetic field of a) 7 Tesla; b) 4.7 Tesla.

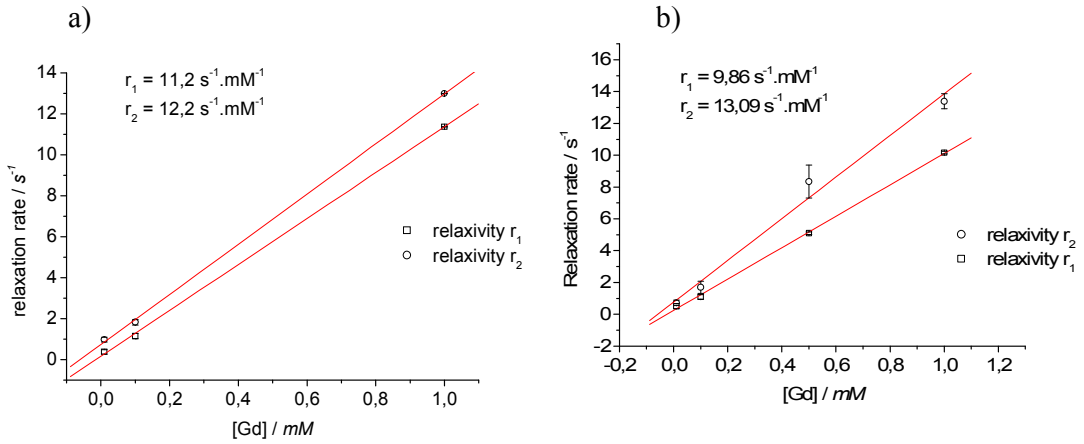

Figure S12. T_1 and T_2 relaxation rate measurements *vs* concentration of aqueous solutions of the nanoparticles a) $Gd^{3+}[Fe(CN)_6]^{3-}$@$PEGNH_2$ **1c;** b) $Gd^{3+}/[Fe(CN)_6]^{3-}$@NADG **1d** performed at an applied magnetic field of 4.7 T.

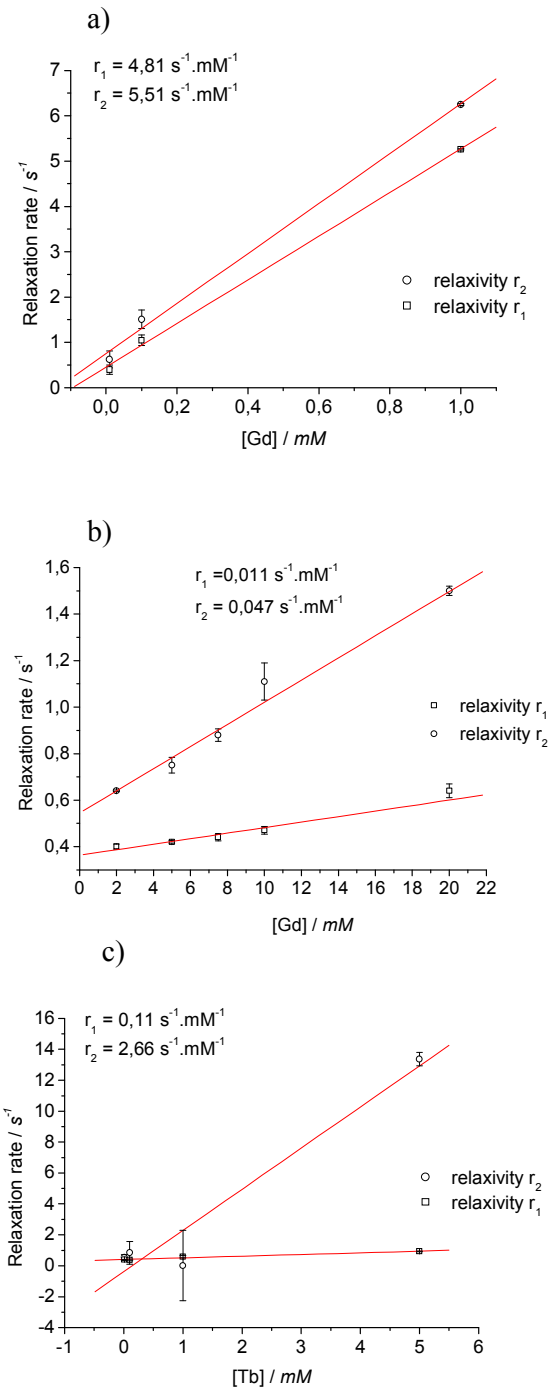

Figure S13. T_1 and T_2 relaxation rate measurements *vs* concentration of aqueous solutions of the nanoparticles a) $Gd^{3+}/[Co(CN)_6]^{3-}$@PEG400 **2;** b) $Y^{3+}/[Fe(CN)_6]^{3-}$@PEG400 **4;** c) $Tb^{3+}/[Fe(CN)_6]^{3-}$@PEG400 **3** performed with an applied magnetic field of 4.7 T.

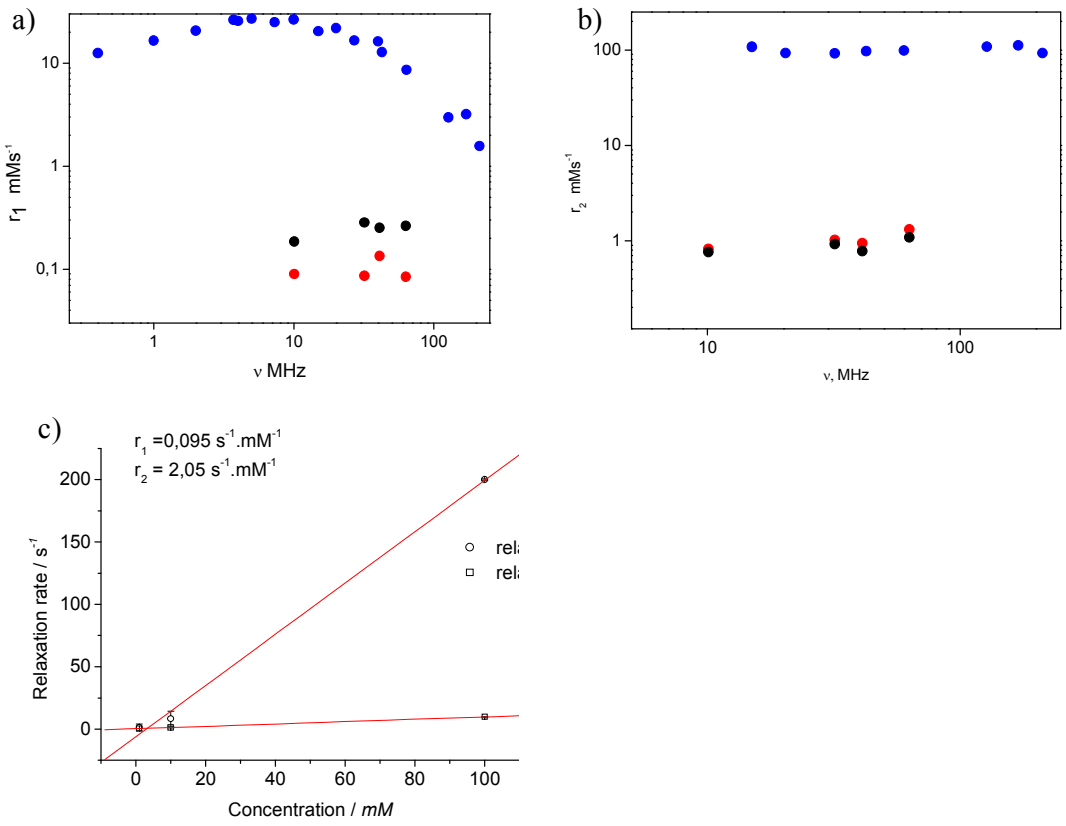

Figure S14. a) Longitudinal and b) Transverse relaxivities for samples **5** (●) and **6** (●) collected at T≈25 °C and compared to the commercial CA Endorem® (●).

c) T_1 and T_2 relaxation rate measurements *vs* concentration of aqueous solutions of the nanoparticles **7** performed at an applied magnetic field of 4.7 T.

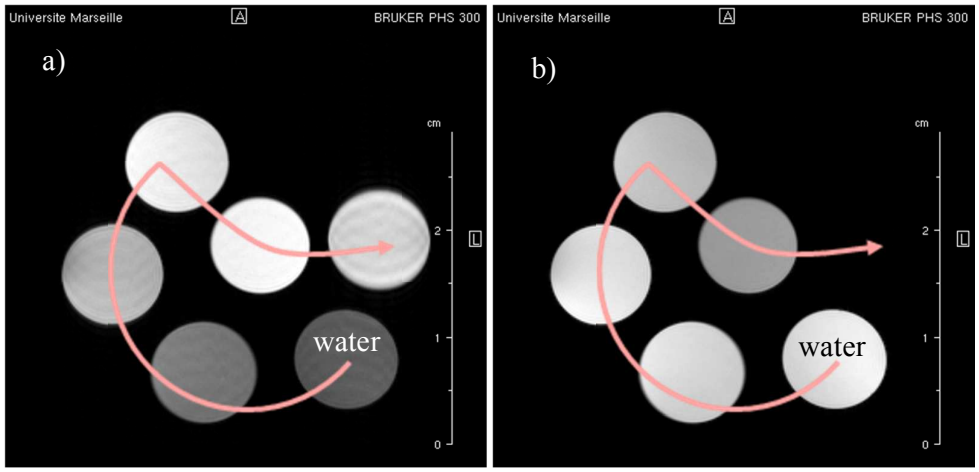

Figure S15. a) T_1-weighted MRI phantoms slices of aqueous solutions of **7** with different concentration. The arrow indicates the direction of increasing concentration; b) T_2-weighted MRI phantoms slices of aqueous solutions of **7** with different concentration. The arrow indicates the direction of increasing concentration. The used concentrations are 0, 0.002, 0.005, 0.0075, 0.01 and 0.015 M.

References:

(1) Cotton, S.; "Lanthanide and Actinied Chemisty", Wiley, **2006**.

(2) CrysAlisPro, Agilent Technologies, Vers 1.171.36.24'

(3) SCALE3 ABSPACK scaling algorithm "Empirical absorption correction using spherical harmonics, implemented in SCALE3 ABSPACK scaling algorithm."

(4) Burla, M. C., Caliandro, R., Camalli, M., Carrozzini, B., Cascarano, G.L., De Caro, L., Giacovazzo, C., Polidori, G. & Spagna, R. (**2005**). SIR2004. An improved tool for crystal structure determination and refinement. *J. Appl. Cryst.* 38, 381.

(5) Sheldrick, G.M. (1997). SHELXL-97. Program for Crystal Structure Refinement. University of Gottingen, Germany.

(6) WinGX version 2013.3 (july 2013), L. J. Farrugia, *J. Appl. Cryst.* 2012,**45**, 849.

(7) Vargas, J. M.; Nunes, W. C.; Socolovsky, L. M.; Knobel, M.; Zanchet, D. *Phys. Rev. B* **2005**, *72*, 184428.

(8) Mydosh, J. A.; *Spin Glasses*, Taylor and Francis, Washington DC, **1993**.